iEnergy

ARTICLE

https://doi.org/10.23919/IEN.2023.0034

Estimating battery state of health with 10-min relaxation voltage across various charging states of charge

Xinhong Feng[1], Yongzhi Zhang[1] ✉, Rui Xiong[2] ✉ and Aihua Tang[3]

ABSTRACT

Battery capacity assessment is a crucial research direction in the field of lithium-ion battery applications. In the previous research, a novel data-driven state of health (SOH) estimation method based on the voltage relaxation curve at full charging is developed. The experimental results have shown the evidence of the superiority of accurate battery SOH estimation based on physical features derived from equivalent circuit models (ECMs). However, the earlier research has limitations in estimating battery capacity with a diversity of battery charging states of charge. This study represents an extension of the previous work, aiming to investigate the feasibility of this technology for battery degradation evaluation under various charging states so that the application capability in practice is enhanced. In this study, six ECM features are extracted from 10-min voltage relaxation data across varying charging states to characterize the battery degradation evolution. Gaussian process regression (GPR) is employed to learn the relationship between the physical features and battery SOH. Experimental results under 10 different state of charge (SOC) ranges show that the developed methodology predicts accurate battery SOH, with a root mean square error being 0.9%.

KEYWORDS

Battery state of health, 10-min relaxation voltage, varying charging states, physical features, machine learning.

Lithium-ion (Li-ion) batteries have emerged as a cornerstone of energy storage solutions, powering an array of applications like smartphones, electric vehicles (EVs) and renewable energy systems[1,2]. These versatile power sources have revolutionized the way people function in daily lives and even reshaped entire industries. However, a fundamental challenge associated with Li-ion batteries is their gradual degradation over time, which inevitably impacts their performance and capacity[3,4]. This ongoing wear and tear can lead to reduced energy storage capabilities and, in some cases, safety concerns. To address these issues and maximize the operational efficiency of devices relying on Li-ion batteries, accurate estimation of battery state of health (SOH) is imperative. SOH serves as a critical parameter in assessing a battery's health and remaining capacity[5,6]. It not only influences the reliability of consumer electronics but also plays a pivotal role in the optimization of electric vehicles' driving range and the stability of renewable energy systems.

Currently, numerous precise methods for battery SOH estimation have emerged, broadly categorized into model-based and data-driven approaches[7,8]. Model-based methods[9,10] entail a manual analysis of the relationship between external factors and battery aging, followed by the modeling of this connection. However, this modeling process is intricate, and normally, models for different types of batteries are not interchangeable, which amplifies the cost in practical applications. Data-driven methods[11–13] employ machine learning models to learn the relationship between battery SOH and health indicators (HIs) extracted from external data. Compared to model-based approaches, data-driven methods are less complex to implement, and the HIs used are easier to obtain in practice. Therefore, they hold greater promise for practical applications. Many studies have achieved favorable SOH estimation results through data-driven methods. Among various raw data sources used for HIs extraction, the relaxation voltage curve in charging is considered relatively accessible. In our previous research[14], we extracted six physical features from battery relaxation voltage at full charging to indicate battery degradation evolution, and based on which, a Gaussian process regression (GPR)-based model was developed for accurate battery SOH estimation. However, the application of the method requires a full charge of the battery, which limits its applicability in practice. To address this limitation, this paper extends the previous methodology by experimentally validating that this method can be applied to accurately estimate battery SOH under varying charging states of charge, thus further enhancing its practicality.

The main content of each section in this paper is as follows. Section 1 provides a detailed description of the process for generating experimental data. Section 2 introduces the method framework developed for battery SOH estimation. Section 3 presents the experimental and validation results, and Section 4 concludes this paper.

1 Experiment

This study employs a dataset obtained from 20 commercial Panasonic NCR18650BD cells, which was originally generated from Ref. [15]. These cells consist of $Li(NiCoAl)O_2$ as the main positive electrode material and graphite as the main negative electrode material. The upper and lower cut-off voltages for these cells are set at 4.2 V and 2.5 V, respectively. According to the manufacturer's specifications, the cell exhibits a nominal capacity of 3.03 Ah when discharged at a rate of 0.606 A at 25 °C, with a nominal voltage of 3.6 V. The experimental procedure is summarized as

[1]College of Mechanical and Vehicle Engineering, Chongqing University, Chongqing 400030, China; [2]Department of Vehicle Engineering, School of Mechanical Engineering, Beijing Institute of Technology, Beijing 100081, China; [3]School of Vehicle Engineering, Chongqing University of Technology, Chongqing 400054, China

Address correspondence to Yongzhi Zhang, yongzhi@cqu.edu.cn; Rui Xiong, rxiong@bit.edu.cn

follows.

On the Arbin BT-5HC battery tester, 20 cells underwent cycling testing across 10 different state of charge (SOC) ranges, yielding the corresponding relaxation voltage curves used for HIs extraction. Table 1 displays the 10 SOC ranges with different start and end SOC values, with the SOC calculated using coulomb counting. The SOC was set to 100% after a constant current–constant voltage (CCCV) charge to 4.2 V, and 0% after a constant current (CC) discharge to 2.5 V. For cells with 0% SOC_{start}, they first underwent CC discharge to 0% SOC, then cycling between SOC_{start} and SOC_{end} with CC charging and discharging. For other cells, they were first charged to 100% SOC, then discharged to the corresponding SOC_{start} and substantially cycled between SOC_{start} and SOC_{end}. During the cycling, the ambient temperature was maintained at 30 °C, with the CC charging current set to 0.3 C-rate (C) and the CC discharging current set to 1 C. There is a 10-min resting between the discharging and charging phases, during which period the voltage relaxation data was collected for features extraction.

Table 1 SOC cycling ranges and corresponding number of cells

SOC_{start}	SOC_{end}	Number of cells
0%	20%	2
20%	30%	2
0%	50%	2
40%	60%	2
25%	75%	2
10%	90%	2
0%	100%	2
50%	100%	2
80%	100%	2
90%	100%	2

The capacity tests were interspersed with cycling to periodically calibrate the current capacity of the battery for SOC calculations. Initially, the cell's capacity was calibrated every 10 days. After several months of cycling tests, it was observed that the capacity was decreasing almost linearly, and therefore, the calibration frequency was then reduced to once in 20 days. The battery capacity calibration procedure is as follows. First, the battery was charged under CCCV at 0.3 C until 4.2 V with a cut-off current of 0.02 C. Then, after one hour of rest, the battery was discharged under CC to 2.5 V at 0.2 C, followed by another hour of rest before another calibration. This process is repeated twice, with the second discharge capacity recorded as the battery calibration capacity.

Figure 1 shows the battery SOH decline trajectories under different SOC ranges, with the SOH values at other cycles interpolated with cubic splines to generate enough amounts of data for machine learning. Generally, Figure 1 shows that the battery degrades faster with larger SOC swing ranges, with the batteries cycled under 0%–100% SOC degrading the fastest. For the battery cells cycled under the same SOC range, the degradation trajectories are similar to each other with some differences.

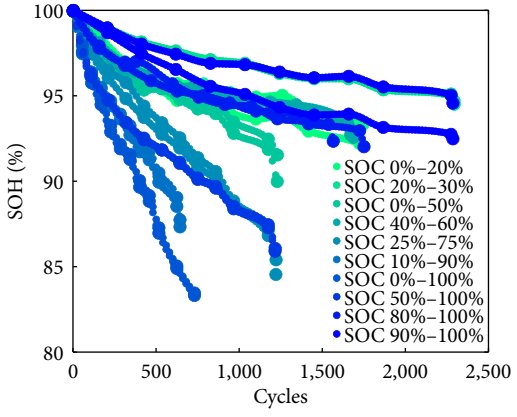

Fig. 1 Battery SOH decline trajectories under different SOC ranges.

2 Methodology

The methodology framework of this study is depicted in Figure 2. The battery's relaxation voltage curves under varying charging states are extracted to capture the battery aging evolution, and based on which, an equivalent circuit model (ECM) is used to identify the six physical features for battery SOH estimation. Then, the relationship between the physical features and battery SOH is constructed by using GPR. Detailed descriptions of the methodology are presented as follows.

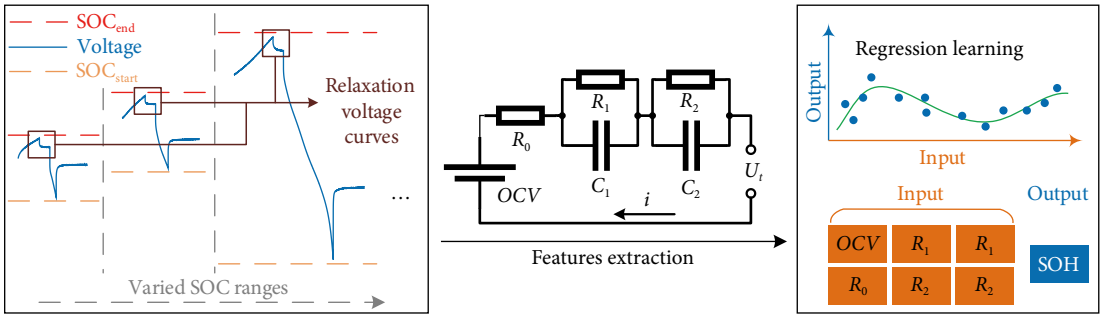

Fig. 2 The framework of the methodology in this study.

2.1 Features extraction

The second-order resistor-capacitor (RC) model (as expressed in Figure 2) is used to extract the key information linked to battery aging based on the relaxation voltage data, and it includes six parameters: the open circuit voltage (*OCV*), the ohmic resistance (R_0), the first-orderpolarization resistance (R_1), the second-order polarization resistance (R_2), the first-order polarization capacitance (C_1), and second-order polarization capacitance (C_2). *OCV* reflects the disparity in Li-ion concentration between the positive and negative electrodes of the battery in a stable state. R_0 signifies the

ohmicpolarization, denoting a voltage drop caused by the physical resistance of the electrodes, electrolyte, and separator. R_1 and C_1 represent the activation polarization during the charge transfer process.R_2 and C_2 correspond to the concentration polarization of lithium ions during the solid-phase diffusion.

Based on the above ECM, the formula for the terminal voltage of the cell is obtained:

$$U_t(t) = OCV - i(t)R_0 - U_1(t) - U_2(t), \tag{1}$$

where U_t and i denote the terminal voltage and the current (positive in discharging), respectively; U_1 and U_2 represent the potential differences across the two RC loops, and t is the time moment. When the cell is at rest, the current is 0 A, thus U_1 and U_2 could be calculated by:

$$U_1(t) = IR_1 e^{-\frac{t}{R_1C_1}}, \tag{2}$$

$$U_2(t) = IR_2 e^{-\frac{t}{R_2C_2}}, \tag{3}$$

where $I = i(0)$ represents the cut-off current before battery relaxation. Combining Eqs. (2) and (3) into Eq. (1) yields the voltage expression of the cell at rest as

$$U_t(t) = OCV - IR_1 e^{-\frac{t}{R_1C_1}} - IR_2 e^{-\frac{t}{R_2C_2}}. \tag{4}$$

The parameters of OCV, R_1, R_2, C_1, and C_2 are obtained by fitting Eq. (4) to the relaxation voltage data under different charging states by using nonlinear fitting techniques (such as but not limited to the least squares method). Then R_0 is calculated with the following derivation:

$$R_0 = \left|\frac{U_t(0) - OCV}{I}\right| - R_1 - R_2. \tag{5}$$

2.2 Gaussian process regression

The GPR is selected as the machine learning method to map the relationship between the extracted features and battery SOH. In GPR, each sample $f(x)$ is assumed to follow a Gaussian distribution with a mean $m(x)$ and covariance $\kappa(x, x')$:

$$f(x) \sim \mathrm{GP}(m(x), \kappa(x, x')), \tag{6}$$

$$m(x) = \mathbb{E}[f(x)], \tag{7}$$

$$\kappa(x, x') = \mathbb{E}\left[(f(x) - m(x))(f(x') - m(x'))^{\mathrm{T}}\right]. \tag{8}$$

Based on this assumption, the training set forms a joint Gaussian distribution. Combined with the conditional probability formula, the posterior predictive distribution of the test sample is obtained.

The kernel function plays a crucial role in GPR and significantly influences the model's performance. The exponential kernel, chosen for its capacity to deliver robust nonlinear regression performance, was used in this study. For two input points, x_i and x_j, the exponential kernel is expressed as:

$$k_{\mathrm{EXP}}(x_i, x_j) = \sigma_f^2 \exp\left(-\frac{1}{\sigma_l}\sqrt{(x_i - x_j)^{\mathrm{T}}(x_i - x_j)}\right), \tag{9}$$

where σ_f and σ_l represent the signal standard deviation and the characteristic length scale, respectively. The values of hyperparameters $\boldsymbol{\theta} = \{\sigma_f, \sigma_l\}$ are optimized by minimizing the negative log marginal likelihood, with the "fitrgp" function in MATLAB.

The root mean square error (RMSE) is employed to measure the estimation error on the testing set, calculated as follows:

$$RMSE = \sqrt{\frac{1}{n}\sum_{i=1}^{n}(y_i - \hat{y}_i)^2}, \tag{10}$$

where n is the number of samples, y_i is the true value, and $\hat{y}_i$ is the estimated value.

3 Results

3.1 Features extraction

The features extracted from ECM have been demonstrated to contain physical and chemical information inside the cell[16]. The voltage response of the battery is resulted from the combined effects of ohmic, activation, and concentration depolarization processes, with the magnitude of each process, quantitively described by the parameters of R_0, R_1, and R_2 of ECM. Additionally, the time constants $\tau_1 = R_1C_1$ and $\tau_2 = R_2C_2$ characterize the rates of the latter two depolarization processes, with the larger values indicating the slower diffusion rates. And the OCV indicates the cell's balance potential between the two electrodes.

Figure 3 displays the ECM features extracted from the 10-min relaxation voltage data at different SOC_{end} values. It is observed that the internal resistances R_0, R_1, and R_2 generally increase while the capacitances C_1 and C_2 decrease as the battery fades, indicating the intensification of the polarization. Note that in some cases, the internal resistances decrease a little at the early stage of battery aging. This phenomenon is attributed to the electrolyte filling the small gaps between electrode particles at the early life stage of the battery, thus expanding their internal contacts and electron-ion transfer paths[16].

As shown in Figure 3, each feature exhibits a generally monotonous changing trend as the battery SOH declines. Note that the OCV trajectories differentiate for different SOC_{end} values, which aid the model in learning the battery aging information at the corresponding SOC values and thereby improves its prediction accuracy. There are some overlaps for the values of other features (R_0, e.g.,) at different SOH points and SOC ranges, which might cause the model unable to differentiate these samples and thus decrease its prediction accuracy. Therefore, it is important to involve the feature OCV for improving the model prediction accuracy. In Figure 3, it is observed that for the batteries cycled with 100% SOC_{end}, different SOC_{start} values make a significant impact on the variation patterns of the features, which phenomenon was generally overlooked in previous research.

3.2 SOH estimation

Figure 4 illustrates the average RMSEs of the five-fold cross-validation results using GPR with different combinations of the six features as input. Note the training and test data are selected from the whole experimental aging data of batteries. For the convenience of display, the numbers from 1 to 6 are used to represent the features OCV, R_0, R_1, R_2, C_1, and C_2, respectively. Figure 4(a) shows the average RMSEs, with the corresponding combination of features presented in Figure 4(b). It is observed that the best battery SOH estimation results based on 1 to 6 features' input are, respectively, obtained with the feature sets of $\{OCV\}$, $\{OCV, R_2\}$, $\{OCV, R_0, R_2\}$, $\{OCV, R_0, R_1, R_2\}$, $\{OCV, R_0, R_1, R_2, C_2\}$, $\{OCV, R_0, R_1, R_2, C_1, C_2\}$, which are highlighted in bold in Figure 4(b). These results indicate the importance levels for different features, which can be roughly ordered from the most to the less importance as OCV, R_2,

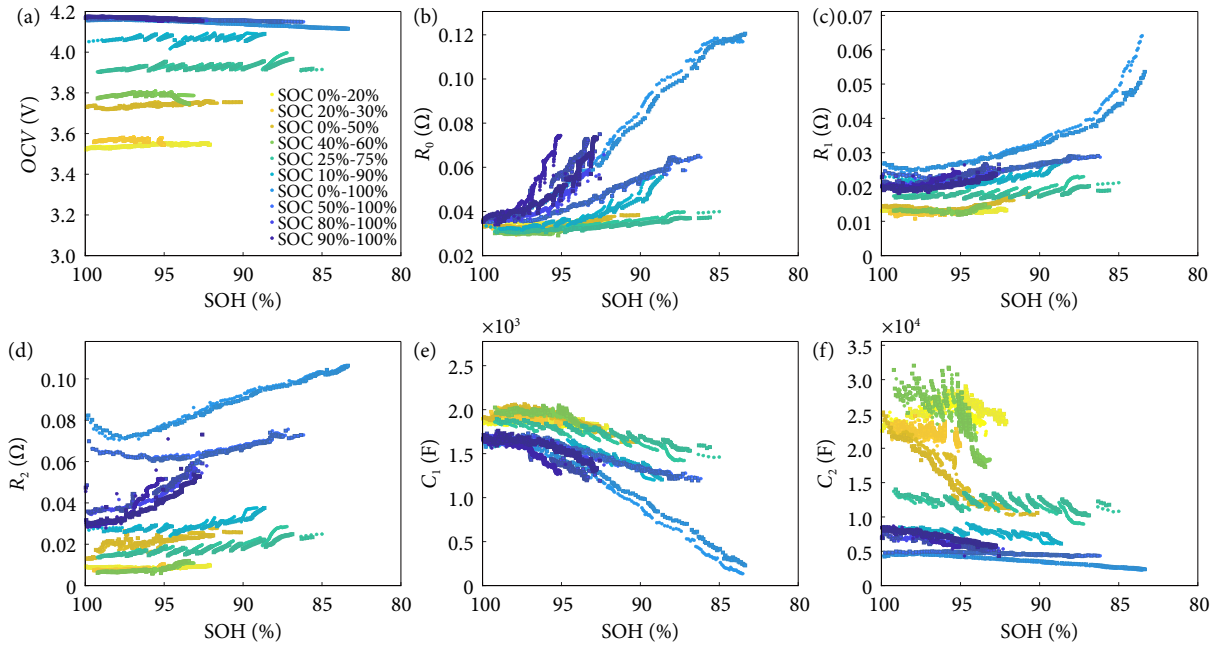

Fig. 3 Features extraction results versus battery SOH. Features of **(a)** *OCV*, **(b)** R_0, **(c)** R_1, **(d)** R_2, **(e)** C_1, and **(f)** C_2.

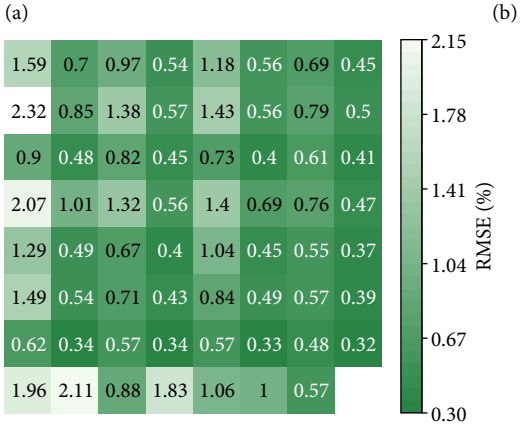

(b)

1	**1,4**	1,5	1,4,5	1,6	1,4,6	1,5,6	1,4,5,6
2	2,4	2,5	2,4,5	2,6	2,4,6	2,5,6	2,4,5,6
1,2	**1,2,4**	1,2,5	1,2,4,5	1,2,6	1,2,4,6	1,2,5,6	1,2,4,5,6
3	3,4	3,5	3,4,5	3,6	3,4,6	3,5,6	3,4,5,6
1,3	1,3,4	1,3,5	1,3,4,5	1,3,6	1,3,4,6	1,3,5,6	1,3,4,5,6
2,3	2,3,4	2,3,5	2,3,4,5	2,3,6	2,3,4,6	2,3,5,6	2,3,4,5,6
1,2,3	**1,2,3,4**	1,2,3,5	1,2,3,4,5	1,2,3,6	**1,2,3,4,6**	1,2,3,5,6	**1,2,3,4,5,6**
4	5	4,5	6	4,6	5,6	4,5,6	

Fig. 4 GPR-based RMSEs of SOH estimation with different feature combinations. (a) Average RMSEs of the five-fold cross-validation. **(b)** The features employed for model training, where the features *OCV*, R_0, R_1, R_2, C_1, and C_2, are represented by the number 1, 2, 3, 4, 5, and 6, respectively.

R_0, R_1, C_2, and C_1. Consistent with the analysis made in Section 3.1, it is observed that, among the single feature-based estimation results, GPR based on *OCV* estimates battery SOH most accurately. Furthermore, it shows that *OCV* is always included in the feature set of estimating accurate battery SOH. As hypothesized earlier, the other features, due to their limited capability in indicating battery aging under different SOC ranges, struggle to obtain satisfactory estimation results when used as the only model input. Generally, the best estimation result with 0.32% RMSE, is obtained based on GPR that utilizes all six features as input, demonstrating that all features contribute to improving the model prediction accuracy.

Figure 5 presents the comparison results of SOH estimation based on different methods, where Figure 5(a) shows the estimation results based on the six physical features while Figure 5(b) shows the results based on six statistical features proposed in Ref. [12], which represents one of the best in indicating reliable and accurate battery degradation in the literature. In this case, the ratio of training and test data is set to 1:1. That is, only one cell from each SOC cycling range is randomly selected, with all their cycling data used for training the GPR model, while the remaining cells' data serve as the test data set for model validation. This data splitting strategy, although influenced by the battery inconsistencies, would better align with the practical application scenarios compared to the five-fold cross-validation. Figure 5(a) shows that, the estimated SOH values under different SOC cycling ranges are close to the observed values, demonstrating the model's generalization capability of estimating SOH upon random charging data. The errors are mainly concentrated between −2% and 2% (as shown in the embedded plot), and the RMSE of the test set's estimation results is 0.9%, confirming the model's high prediction accuracy.

The six statistical features include the maximum (*Max*), mean (*Mean*), minimum (*Min*), variance (*Var*), skewness (*Ske*), and kurtosis (*Kur*), which are also extracted from the 10-min voltage relaxation data for fair comparisons. The formulas to calculate these statistical features are referred to Ref. [12]. A GPR model was also developed based on the six statistical features for battery SOH estimation. Figure 5(b) illustrates that the estimation RMSE is 1.03%, which is higher than that based on physical features. And some estimations under 10%–90% SOC cycling range significantly

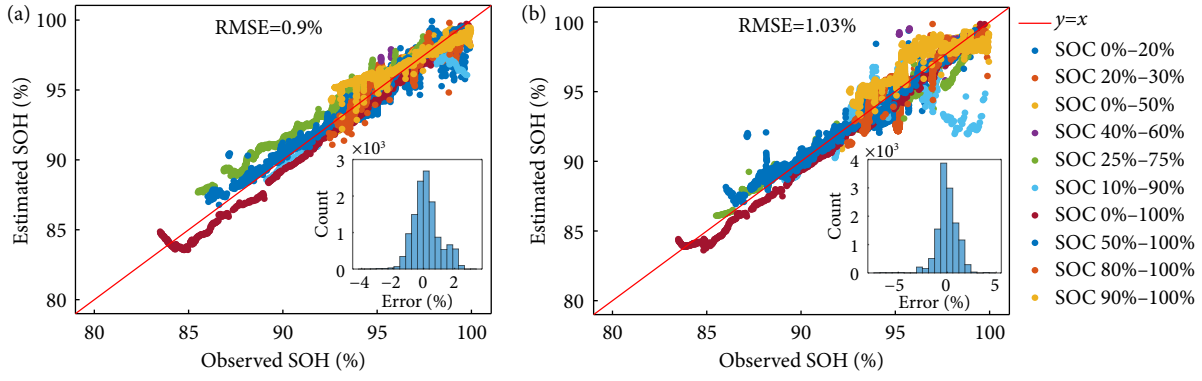

Fig. 5 SOH estimation results based on features of (a) *OCV*, R_0, R_1, R_2, C_1, and C_2; (b) *Max*, *Mean*, *Min*, *Var*, *Ske*, and *Kur*.

deviate from the observed values (as shown in the embedded plot), further demonstrating the superiority of the physical features in indicating reliable battery degradation evolution.

4 Conclusions

Battery state of health (SOH) is a crucial parameter for assessing the extent of battery degradation. In the previous research, we have extracted six physical features from the battery relaxation voltage at full charging and constructed a machine learning model based on Gaussian process regression (GPR) to predict accurate battery SOH under different operating scenarios. In this study, we further extend the methodology to estimate battery SOH under different SOC ranges to further enhance its feasibility in practice.

This paper introduces an SOH estimation method capable of adapting to different battery charging states of charge. The methodology framework is mainly based on the previous research, where the parameters of an equivalent circuit model are identified based on the voltage relaxation data and used as physical features to indicate battery degradation. Then, the GPR is used to learn this relationship between the physical features and battery SOH. This study introduces more aging data of batteries to validate the model performance of estimating battery SOH under varying SOC cycling ranges. The cross-validation results indicate the importance of the *OCV* feature in improving the model accuracy with changeable SOC cycling ranges, and it is important to involve in all six physical features to estimate accurate battery SOH. Experimental results show that the method estimates battery SOH accurately with a root mean square error of 0.9%, which accuracy is higher than that of the model based on statistical features, validating the superiority of the developed method in battery SOH estimation using random partial charging data.

This paper demonstrates an important extension of a recently published methodology, which greatly improves the potential of the method to be deployed into the battery management system and is expected to enlighten new thoughts of the researchers in the field.

Acknowledgements

This work was supported by the National Natural Science Foundation of China (No. 52307234) and Beijing Natural Science Foundation (Grant No. L223013). The systemic experiments of the lithium-ion batteries were performed at the Joint Lab for Advanced Energy Storage and Applications, Beijing Institute of Technology.

Author contributions

Xinhong Feng: Methodology, Modeling, Presentation, Writing-original draft. Yongzhi Zhang: Conceptualization, Supervision, Methodology, Writing-original draft, reviewing and editing. Rui Xiong: Conceptualization, Supervision, Writing-reviewing and editing. Aihua Tang: Supervision, Writing-reviewing and editing.

Article history

Received: 10 July 2023; Revised: 23 September 2023; Accepted: 29 October 2023

Additional information

Declaration of competing interest

The authors have no competing interests to declare that are relevant to the content of this article.

References

[1] Frith, J. T., Lacey, M. J., Ulissi, U. (2023). A non-academic perspective on the future of lithium-based batteries. *Nature Communications*, 14: 420.

[2] He, H., Sun, F., Wang, Z., Lin, C., Zhang, C., Xiong, R., Deng, J., Zhu, X., Xie, P., Zhang, S., et al. (2022). China's battery electric vehicles lead the world: Achievements in technology system architecture and technological breakthroughs. *Green Energy and Intelligent Transportation*, 1: 100020.

[3] Zhang, Y., Zhao, M. (2023). Cloud-based *in situ* battery life prediction and classification using machine learning. *Energy Storage Materials*, 57: 346–359.

[4] Zhou, Z., Liu, Y., You, M., Xiong, R., Zhou, X. (2022). Two-stage aging trajectory prediction of LFP lithium-ion battery based on transfer learning with the cycle life prediction. *Green Energy and Intelligent Transportation*, 1: 100008.

[5] Zhang, Y., Feng, X., Zhao, M., Xiong, R. (2023). *In-situ* battery life prognostics amid mixed operation conditions using physics-driven machine learning. *Journal of Power Sources*, 577: 233246.

[6] Aitio, A., Howey, D. A. (2021). Predicting battery end of life from solar off-grid system field data using machine learning. *Joule*, 5: 3204–3220.

[7] Roman, D., Saxena, S., Robu, V., Pecht, M., Flynn, D. (2021). Machine learning pipeline for battery state-of-health estimation. *Nature Machine Intelligence*, 3: 447–456.

[8] Elmahallawy, M., Elfouly, T., Alouani, A., Massoud, A. M. (2022).

A comprehensive review of lithium-ion batteries modeling, and state of health and remaining useful lifetime prediction. *IEEE Access*, 10: 119040–119070.

[9] Schimpe, M., Edler von Kuepach, M., Naumann, M., Hesse, H. C., Smith, K., Jossen, A. (2018). Comprehensive modeling of temperature-dependent degradation mechanisms in lithium iron phosphate batteries. *Journal of the Electrochemical Society*, 165: A181.

[10] O'Kane, S. E. J., Ai, W., Madabattula, G., Alonso-Alvarez, D., Timms, R., Sulzer, V., Edge, J. S., Wu, B., Offer, G. J., Marinescu, M. (2022). Lithium-ion battery degradation: How to model it. *Physical Chemistry Chemical Physics*, 24: 7909–7922.

[11] Lin, C., Xu, J., Hou, J., Liang, Y., Mei, X. (2023). Ensemble method with heterogeneous models for battery state-of-health estimation. *IEEE Transactions on Industrial Informatics*, 19: 10160–10169.

[12] Zhu, J., Wang, Y., Huang, Y., Bhushan Gopaluni, R., Cao, Y., Heere, M., Mühlbauer, M. J., Mereacre, L., Dai, H., Liu, X., et al. (2022). Data-driven capacity estimation of commercial lithium-ion batteries from voltage relaxation. *Nature Communications*, 13: 2261.

[13] Zhao, Y., Wang, Z., Sun, Z., Liu, P., Cui, D., Deng, J. (2023). Data-driven lithium-ion battery degradation evaluation under overcharge cycling conditions. *IEEE Transactions on Power Electronics*, 38: 10138–10150.

[14] Feng, X., Zhang, Y., Xiong, R., Wang, C. (2023). Comprehensive performance comparison among different types of features in data-driven battery state of health estimation. *arXiv preprint*, 2308.13993.

[15] Zhang, Y., Xiong, R., He, H., Qu, X., Pecht, M. (2019). State of charge-dependent aging mechanisms in graphite/Li(NiCoAl)O_2 cells: Capacity loss modeling and remaining useful life prediction. *Applied Energy*, 255: 113818.

[16] Qian, K., Huang, B., Ran, A., He, Y. B., Li, B., Kang, F. (2019). State-of-health (SOH) evaluation on lithium-ion battery by simulating the voltage relaxation curves. *Electrochimica Acta*, 303: 183–191.